Eur. Phys. J. Plus (2019) **134**: 320
DOI 10.1140/epjp/i2019-12644-8

THE EUROPEAN PHYSICAL JOURNAL PLUS

Regular Article

Electromechanical stability analysis of smart double-nanobeam systems

Reza Bahaadini[1], Mohammad Hosseini[2,a], and Zahra Khalili-Parizi[2]

[1] Department of Mechanical Engineering, Shahid Bahonar University of Kerman, Kerman, I.R. Iran
[2] Department of Mechanical Engineering, Sirjan University of Technology, Sirjan 78137-33385, I.R. Iran

Received: 7 October 2018 / Revised: 24 January 2019
Published online: 8 July 2019

Abstract. In the present article, the electromechanical stability analysis of double-nanobeam-systems (DNBS) under subtangential forces is studied based on Eringen's nonlocal elasticity theory. The two cantilever nanobeams are assumed parallel and coupled by an enclosing visco-Pasternak medium. Furthermore, each nanobeam is surrounded by two piezoelectric layers and the system resting on Winkler elastic medium. The governing equations of motion and associated boundary conditions are derived by the extended Hamilton's principle. Applying the extended Galerkin's approach, the partial differential equations are transformed to ordinary differential equations. The effects of the nonlocal parameter, piezoelectric voltage, aspect ratios and surface effects on the vibration and stability characteristics of the DNBS are explained in detail. It is observed that the critical flutter and divergence loads predicted by the classical continuum theory have more value than the nonlocal continuum theory. In order to validate the accuracy and applicability of the proposed model, the numerical results are confirmed by comparing the results with those obtained in the literature.

1 Introduction

Divergence instability is the only kind of instability that can occur in a conservative system. However, in non-conservative systems both divergence and flutter instabilities are possible. Beams and columns are slender structural components that affect these kinds of instabilities, so, a cantilever beam under the action of subtangential forces is a simple example of non-conservative system, which received a great deal of attention among researchers and is extensively used in many field of study like aerospace structures, tall building and aeronautical engineering applications. From the above-mentioned statements, Zuo and Schreyer [1] studied the divergence and flutter instabilities of beams and plates subjected to a subtangential force. Langthjem and Sugiyama [2,3] analysed the optimization problem of damped and undamped cantilever columns under a subtangential force. A mathematical modeling along with the integral equation formulation was utilized to investigate the flutter and divergence instability of beams by Elfelsoufi and Azrar [4]. Şimşek and Cansız [5] focused on the dynamic responses of an elastically connected double-functionally graded beam systems (DFGBS) with elastically restrained edges subjected to a moving harmonic load with a constant speed. Mao and Wattanasakulpong [6] employed the Adomian modified decomposition method (AMDM) to investigate the free vibration and stability analysis of a cantilever double-beam system, which is interconnected by a Winkler-type elastic layer under a subtangential force. The dynamic responses of a double-beam system under compressive axial load, which are caused by arbitrarily distributed continuous loads have been discussed by Zhang *et al.* [7]. Moreover, the conservative and non-conservative instability of structures can be found in the work of refs. [8–18].

Since the classical continuum theory is not able to describe the dependence of the mechanical behavior of micro/nanoscale structures on the size effect, the extended methods become essential to predict the nanoscale effects. According to the nonlocal elasticity theory, the stress state at a reference point is a function of the strain states of all points in the domain [19–26]. Hence, due to the recent developments in science and technology, nano/micro structures have held wide applications in nanoelectromechanical systems (NEMS), microelectromechanical systems (MEMS), mass sensors and nanoactuators. Based on the nonlocal elasticity theory, the bending, buckling and vibration of various beams have been analyzed by Reddy [27]. Bahaadini and Hosseini [28] described the effects of nonlocal parameter, structural damping coefficients, Knudsen number and mass ratio on the vibrational frequency and flutter

[a] e-mail: hosseini@sirjantech.ac.ir (corresponding author)

boundary of viscoelastic cantilever carbon nanotubes (CNTs)-conveying fluid. In another work, they investigated the effects of nonlocal parameter, magnetic field, elastic foundation and boundary conditions on the divergence and flutter boundaries of fluid conveying CNTs [28]. Wang and Liew [29] investigated the vibration and buckling of CNTs based on Eringen's nonlocal elasticity theory. Generally, knowing about the dynamic behavior of complex systems might be useful for the development of technology and engineering science. The double-nanobeam systems (DNBS) are one such complex-nanobeam systems, which consist of two one-dimensional nanobeams linked by a coupling medium like Van der Waals forces, elastic medium and so on. It can be noted that one of the most important applications of a DNBS is nano-optomechanical systems (NOMS). In recent years, using nonlocal continuum mechanics, the instability [30, 31], vibration [32–35], vibration and biaxial buckling [36,37], wave propagation [38], dynamics response [39–42] and buckling behavior [43,44] of nanostructures systems have been investigated. Ciekot and Kukla [45] employed Green's function method to study the transverse vibration of DNBS. Recently, Hosseini *et al.* [46] investigated the forced vibration of double piezoelectric micro-pipe conveying fluid under a moving load.

The surface effects are intrinsically size-dependent while the surface-to-volume ratio increases with decreasing size to the nano-scale. Paying attention to the surface energy and/or surface stresses, the influence of surface effects on the mechanical behavior of nanoscale components and nanomaterials can be investigated [47,48]. These authors analyzed the parameters of surface effects including surface elasticity, surface stress and surface density on the natural frequencies of nano-beams. The influence of surface effect on the vibration behaviors of carbon nanotubes under initial stress was studied by Chen *et al.* [50]. Zhang *et al.* [51] analyzed the vibration of viscoelastic nanobeams to study the effects of nonlocal parameter, viscoelastic constants, surface elasticity and residual surface tension.

The applications of new structures including complex- nanobeam systems, which are bonded with piezoelectric actuators, have been widely considered by many researchers in different fields of science and engineering [52]. The piezoelectric materials, as a major group of smart structures, produce an electric field if a deformation is applied to them, and undergo deformation by applying an electric field. So, due to their superior properties, they have received tremendous attention from the research community [53]. In this regard, based on the Timoshenko beam model and the piezoelectricity theory, Zhi and Liying [54] investigated the influence of the flexoelectric effect on the static bending and free vibration of a simply supported nanobeam. Hosseini *et al.* [55] performed a nonlocal piezoelectric carbon-nanotube–conveying fluid to investigate the nonlocal parameter, piezoelectric voltage and surface effects on the divergence and flutter boundaries of the system. Fereidoon *et al.* [56] examined the nonlinear vibration of viscoelastic embedded-DWCNTs integrated with piezoelectric layers conveying viscous fluid by considering surface effects. In the context of the nonlocal piezoelectricity theory, the influences of nonlocal parameter, visco-Pasternak constants, voltage, Kelvin-Voigt and Maxwell coefficients on the vibration behavior of double viscoelastic piezoelectric nanobeam systems was examined by Ghorbanpour-Arani *et al.* [57].

According to the best of our knowledge, no studies have been accomplished on the divergence and flutter boundaries of cantilever smart coupled DNBS embedded in an elastic medium subjected to a subtangential force. The governing equations of motion based on Eringen's nonlocal and Gurtin-Murdoch continuum elasticity theories have been derived. Using the extended Galerkin's approach, the governing equations are changed into a class of eigenvalue equations and solved numerically. The main objective of this study is to predict the influences of nonlocal and non-conservative parameters, piezoelectric voltage, different values of subtangential forces, and surface effects on the critical flutter and divergence loads and the natural frequencies of DNBS.

2 Governing equations

Consider the free vibration of smart DNBS subjected to a subtangential force, as shown in fig. 1. The DNBS resting on the visco-Pasternak foundation, which is simulated by the spring constant of Winkler-type (k_w), the shear constant of Pasternak-type (k_G) and damping coefficient (c). Both nanobeams have the same length L, width b, thickness h_b, density ρ_b and Young's modulus E_b. Here, h_p, ρ_p and E_p are the thickness, density and Young's modulus of the piezoelectric layers, respectively. Also, the surface properties of two inner and outer surface layers are considered to have Lamé surface constants λ_s and μ_s, mass density ρ_s and surface residual tension τ_s.

2.1 Theoretical formulation

With respect to the classical elasticity theory, the nonlocal elasticity theory incorporates the small-scale effect to consider the influence of the strains of distant points on the reference points x. As a result, the nonlocal elasticity theory assumes that the stress at a reference point is related to the strains at the all points of the domain. The differential form of the nonlocal elasticity theory is indicated by Eringen and Edelen [58] as

$$\left(1-\mu^2\nabla^2\right)\sigma_{kl}=\tau_{kl}, \tag{1}$$

where μ stands for a parameter that represents small-size effects, ∇^2 is the Laplacian operator, σ_{kl} is the nonlocal stress tensor and τ_{kl} stands for the classical stress tensor. Also, the extended form of nonlocal equations for a piezoelectric

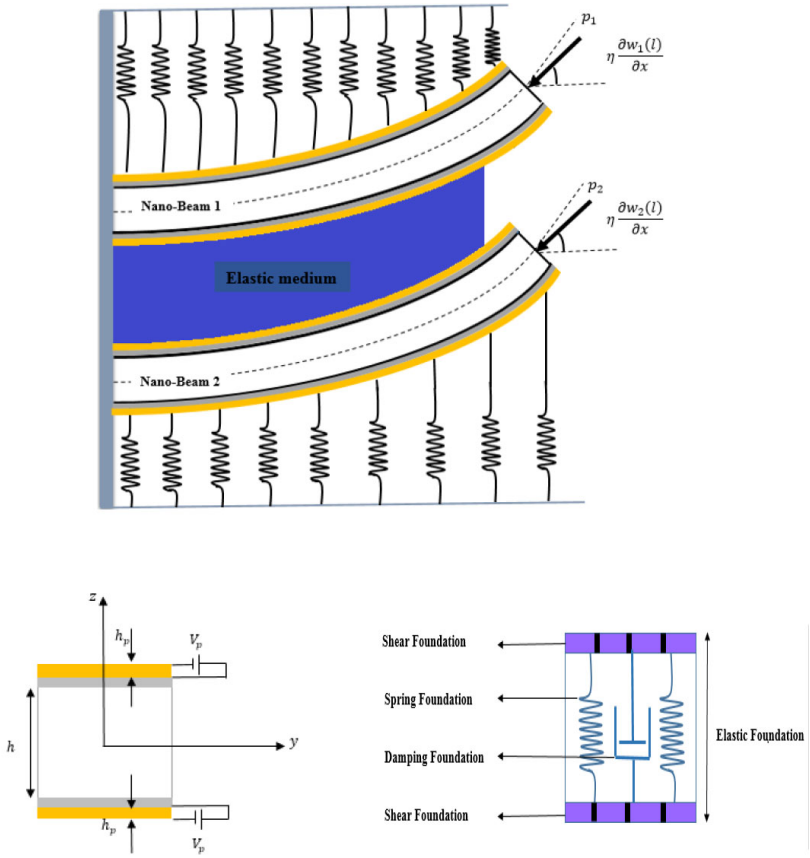

Fig. 1. Non-conservative DNBS actuated by piezoelectric layers and subject to subtangential forces considering the surface effect.

material can be written in differential forms as [59]

$$\left(1-\mu^2\nabla^2\right)\sigma_{kl} = \mathtt{C}_{klmn}\varepsilon_{mn} - e_{mkl}E_m, \tag{2}$$

$$\left(1-\mu^2\nabla^2\right)D_i = e_{ikl}\varepsilon_{kl} + \epsilon_{ik}E_k, \tag{3}$$

where D_i is the electric displacement, E_i is the electric field, $\mathtt{C}_{klmn}$, e_{mkl} and ϵ_{ik} denote elastic constants, piezoelectric constants and dielectric constants, respectively.

Based on the Euler-Bernoulli beam theory, the displacement field and strain relation can be considered as follows when the deformation of mid-plane is negligible:

$$u_1 = -z\frac{\partial w_i(x,t)}{\partial x}, \qquad u_2 = 0, \qquad u_3 = w_i(x,t), \tag{4}$$

$$\varepsilon_{xx} = -z\frac{\partial^2 w_i(x,t)}{\partial x^2}, \tag{5a}$$

$$\varepsilon^p_{xx} = -z\frac{\partial^2 w_i(x,t)}{\partial x^2}, \tag{5b}$$

where the transverse displacement of the i-th nano-beam ($i = 1, 2$) is denoted as $w_i(x,t)$ and ε_{xx} is the only nonzero strain of the Euler-Bernoulli beam theory. Of particular interest is the fact that nanostructure materials have higher surface-to-volume ratio than the conventional ones. Therefore, surface properties can have significant influence on the structural mechanic behavior. Based on Gurtin-Murdoch theory, the stress-strain relations for the surface of i-th nanobeams are given as follows [60,20]:

$$\sigma^s_{xx} = \left(\lambda_s + 2\mu_s\right)\varepsilon_{xx} + \tau^s, \tag{6}$$

$$\sigma^s_{xz} = \tau^s\frac{\partial w_i}{\partial x}. \tag{7}$$

In these relations the superscript s is utilized to denote the relevant quantities of surface. It is noted that the stress component σ^b_{zz} is the smallest stress among σ^b_{xx} and σ^b_{xz} in the classical beam theories. Thus, in order to simplify, σ^b_{zz} can be neglected ($\sigma^b_{zz}=0$). But this assumption is not effective to satisfy the surface conditions considered in the Gurtin-Murdoch theory. To tackle this problem, it is assumed that the stress component σ^b_{zz} varies linearly through the beam thickness and satisfies the balance conditions on the surfaces [61]. So, σ^b_{zz} can be written as follows:

$$\sigma^b_{zz}=\frac{(\frac{\partial\sigma^s_{xz}}{\partial x}-\rho_s\frac{\partial^2 w_i}{\partial t^2})|_{at\ top}-(\frac{\partial\sigma^s_{xz}}{\partial x}-\rho_s\frac{\partial^2 w_i}{\partial t^2})|_{at\ bottom}}{2}+\frac{(\frac{\partial\sigma^s_{xz}}{\partial x}-\rho_s\frac{\partial^2 w_i}{\partial t^2})|_{at\ top}+(\frac{\partial\sigma^s_{xz}}{\partial x}-\rho_s\frac{\partial^2 w_i}{\partial t^2})|_{at\ bottom}}{h_b}z. \quad (8)$$

Using the strain-displacement relations, we can express the nonzero components of stress for the bulk of the i-th nanobeams in terms of displacement as follows:

$$\sigma^b_{xx}=E\varepsilon_{xx}+v\sigma^b_{zz}=-zE\frac{\partial^2 w_i}{\partial x^2}+\frac{2\nu z\tau^s}{h}\left(\tau^s\frac{\partial^2 w_i}{\partial x^2}-\rho^s\frac{\partial^2 w_i}{\partial t^2}\right), \quad (9a)$$

$$\sigma^p_{xx}=c_{11}\varepsilon^p_{xx}-e_{31}E_z, \quad (9b)$$

$$D_z=e_{31}\varepsilon^p_{xx}+\epsilon_{33}E_z, \quad (9c)$$

where v is the Poisson ratio. The internal strain energy of the i-th nano-beam (U) and the strain energy stored in the piezoelectric layers (U_a), because of the axial stress generated by the applied voltage V are expressed as

$$U=U_b+U_p=\frac{1}{2}\left[\int_0^l\int_{A_b}\sigma^b_{ij}\varepsilon_{ij}\mathrm{d}A_b\mathrm{d}x+\left(\int_{S^+}\sigma^s_{ij}\varepsilon_{ij}\mathrm{d}S^+ +\int_{S^-}\sigma^s_{ij}\varepsilon_{ij}\mathrm{d}S^-\right)+\int_0^l\int_{A_p}(\sigma^p_{ij}\varepsilon_{ij}-D_zE_z)\mathrm{d}A_p\mathrm{d}x\right], \quad (10a)$$

$$U_a=\frac{1}{2}\int_0^l p_z\left(\frac{\partial w_i}{\partial x}\right)^2\mathrm{d}x, \quad (10b)$$

where, U_b is the strain energy in a deflected nanobeam incorporating surface effects based on the continuum surface elasticity theory, and U_p is the strain energy in a deflected piezoelectric layer. Also E_z and p_z are defined as

$$E_z=\frac{V}{h_p}\quad\text{and}\quad p_z=-2be_{31}V. \quad (11)$$

Here p_z is the axial force resulted by the applied piezoelectric voltage [62]. Also, σ^b_{ij} and σ^p_{ij} are the stresses in the nanobeams and piezoelectric layers, respectively. The electric displacement and electric field in the piezoelectric layers are denoted as D_z and E_z, respectively. Furthermore, V denotes the value of applied voltage to the piezoelectric layers.

The variations of strain energy are obtained by replacing eq. (5) into eq. (10), as follows:

$$\delta U=\int_0^l\left[-\left(M^b_x+M^p_x+M^s_x\right)\frac{\partial^2\delta w_i}{\partial x^2}+Q^s_x\frac{\partial\delta w_i}{\partial x}\right]\mathrm{d}x, \quad (12)$$

where, Q^s_x is resultant axial force in the x-axis direction due to the existence of surface effects. M^b_x, M^p_x and M^s_x are the resultant bending moments which are defined as

$$M^b_x=\int_{A_b}\sigma^b_{xx}z\,\mathrm{d}A_b,\qquad M^p_x=\int_{A_p}\sigma^p_{xx}z\,\mathrm{d}A_p,\qquad M^s_x=\int_S\sigma^S_{xx}z\,\mathrm{d}s,\qquad Q^s_x=\int_S\sigma^S_{xz}\mathrm{d}s. \quad (13)$$

Using eqs. (2), (3), (6), (7), and (9) along with eqs. (5) and (13) we have

$$M^b_x-\mu^2\frac{\partial^2 M^b_x}{\partial x^2}=(-EI_b+A_{11})\frac{\partial^2 w_i}{\partial x^2}-A_{22}\frac{\partial^2 w_i}{\partial t^2},\quad\text{where } A_{11}=\frac{2\nu I_b}{h_b}\tau^s,\quad A_{22}=\frac{2\nu I_b}{h_b}\rho_s, \quad (14a)$$

$$M^p_x-\mu^2\frac{\partial^2 M^p_x}{\partial x^2}=-C_{11}I_p\frac{\partial^2 w_i}{\partial x^2}-e_{31}QE_z, \quad (14b)$$

$$M^s_x-\mu^2\frac{\partial^2 M^s_x}{\partial x^2}=-D_{11}\frac{\partial^2 w_i}{\partial x^2},\quad\text{where } D_{11}=(\lambda_s+2\mu_s)\left(\frac{A_bh_b}{2}+\frac{h_b^3}{6}\right), \quad (14c)$$

$$Q^s_x-\mu^2\frac{\partial^2 Q^s_x}{\partial x^2}=2b\tau^s\frac{\partial w_i}{\partial x}, \quad (14d)$$

$$D_z-\mu^2\frac{\partial^2 D_z}{\partial x^2}=e_{31}\varepsilon^p_{xx}+\epsilon_{33}E_z. \quad (14e)$$

In the relation (14), $Q = \int_{A_p} z\,\mathrm{d}A_p$ and $I_p = h_p h_b b(\frac{h_b}{2}+h_p)$ are defined as the first and second moment of cross-sectional area of piezoelectric layers with respect to the neutral axis of the nano-beam, respectively. Also $I_b = \int_{A_b} z^2 \mathrm{d}A_b$ is the second moment of cross-sectional area of the nano-beam. Moreover, the variation form of the kinetic energy of the i-th nanobeam incorporating the surface effects and piezoelectric layers can be written as

$$\delta T = -\int_0^l \left(\rho_b A_b + 2b\rho_s + \rho_p A_p\right)\left(\frac{\partial^2 w_i}{\partial t^2}\right)\delta w_i \mathrm{d}x. \tag{15}$$

In addition, the potential energy E_c which includes the work done by the conservative component of the subtangential force and the virtual work δW_{nc} done by the non-conservative component of the force acting at the free end of the i-th nano-beam are considered as follows:

$$E_c = -\frac{1}{2}\int_0^l p_i \left(\frac{\partial w_i}{\partial x}\right)^2 \mathrm{d}x, \tag{16a}$$

$$\delta W_{nc} = -p_i \eta \frac{\partial w_i(l)}{\partial x}\delta w_i(l). \tag{16b}$$

The parameter η is characterized as a non-conservative parameter. Different values of η can describe different instability behavior. Here $\eta = 0$ is termed as the pure compressive axial load, whereas the pure follower load is applied when $\eta = 1$, and both conservative axial and non-conservative follower loads act for the values $0 < \eta < 1$. Also, the variational form of the external work of the Winkler foundation between two nanobeams and the surrounding elastic medium of the i-th nanobeam can be written as

$$\delta V = -\int_0^l q\delta w_i \mathrm{d}x, \tag{17a}$$

$$q = k_w\left(2w_i - w_j\right) - k_G\left(\frac{\partial^2 w_i}{\partial x^2} - \frac{\partial^2 w_j}{\partial x^2}\right) + c_d\left(\frac{\partial w_i}{\partial t} - \frac{\partial w_j}{\partial t}\right), \quad (i,j = 1,2, j \neq i). \tag{17b}$$

Using the extended Hamilton's variational principle, the equations of motion of coupled DNBS tunable with piezoelectric layers and under the action of a subtangential force which is surrounded by means of an elastic medium can be expressed by substituting eqs. (12), (15), (16) and (17) into the following relation:

$$\int_{t_1}^{t_2} \left(\delta T - \delta U - \delta U_a - \delta E_c + \delta V + \delta W_{nc}\right)\mathrm{d}t = 0. \tag{18}$$

Therefore, the governing equation of the i-th nanobeam is obtained as

$$\left(\rho A\right)_{eq}\frac{\partial^2 w_i}{\partial t^2} - \frac{\partial^2 M_{eq}}{\partial x^2} + \left(p_i - p_z - 2b\tau^s\right)\frac{\partial^2 w_i}{\partial x^2} + q = 0. \tag{19a}$$

Also, the boundary conditions extracted from the extended Hamilton's principle for the i-th cantilevered nanobeam by considering surface effects and piezoelectric layers subjected to a subtangential force is written as

$$-M_{eq}\frac{\partial \delta w_i}{\partial x}\bigg|_0^l = 0, \tag{19b}$$

$$\left(\frac{\partial M_{eq}}{\partial x} + \left(p_z + 2b\tau^s - p_i(1-\eta)\right)\frac{\partial w_i}{\partial x}\right)\delta w_i\bigg|_0^l = 0, \tag{19c}$$

where $(\rho A)_{eq} = \rho_b A_b + 2b\rho_s + \rho_p A_p$ is the effective inertia of DNBS. Also, the effective moment of the system, M_{eq}, can be defined as

$$\begin{aligned} M_{eq} = \mu^2 \Bigg[&(\rho A)_{eq}\frac{\partial^2 w_i}{\partial t^2} + \left(p_i - p_z - 2b\tau^s\right)\frac{\partial^2 w_i}{\partial x^2} + k_w(2w_i - w_j) - k_G\left(\frac{\partial^2 w_i}{\partial x^2} - \frac{\partial^2 w_j}{\partial x^2}\right) \\ &+ c_d\left(\frac{\partial w_i}{\partial t} - \frac{\partial w_j}{\partial t}\right)\Bigg] - (cI)_{eq}\frac{\partial^2 w_i}{\partial x^2} - A_{22}\frac{\partial^2 w_i}{\partial t^2}, \end{aligned} \tag{20}$$

where

$$(cI)_{eq} = EI_b - A_{11} + D_{11} + c_{11}I_p. \tag{21}$$

Substituting eq. (20) into eqs. (19), the final form of the governing equation of motion and the associated boundary conditions of the i-th nanobeam can be obtained. Hereafter, to simplify the analysis, the following non-dimensional quantities are defined:

$$X=\frac{x}{L},\qquad W_i=\frac{w_i}{L},\qquad T=\frac{t}{L^2}\left(\frac{EI_b}{\rho_b A_b}\right)^{1/2},\qquad \beta=\frac{\mu}{L},\qquad D_{eq}=\frac{(cI)_{eq}L^3}{EI_b},$$
$$A_{eq}=\frac{(\rho A)_{eq}}{\rho_b A_b},\qquad A_{33}=\frac{2b\tau^s L^2}{EI_b},\qquad a_{22}=\frac{A_{22}}{\rho_b A_b L^2},\qquad P_i=\frac{p_i L^2}{EI_b},$$
$$P_z=\frac{p_z L^2}{EI_b},\qquad K_w=\frac{k_w L^4}{EI_b},\qquad K_G=\frac{k_G L^2}{EI_b},\qquad C_d=\frac{c_d L^2}{(EI_b\rho_b A_b)^{1/2}}. \tag{22}$$

Substituting the above parameters in the governing equations and the corresponding boundary conditions leads to their non-dimensional forms as below:

$$\left\{D_{eq}\frac{\partial^4 W_i}{\partial X^4}+(P_i-P_z-A_{33})\frac{\partial^2 W_i}{\partial X^2}+A_{eq}\frac{\partial^2 W_i}{\partial T^2}+a_{22}\frac{\partial^4 W_i}{\partial X^2\partial T^2}+K_w(2W_i-W_j)-K_G\left(\frac{\partial^2 W_i}{\partial X^2}-\frac{\partial^2 W_j}{\partial X^2}\right)\right.$$
$$+C_d\left(\frac{\partial W_i}{\partial T}-\frac{\partial W_j}{\partial T}\right)-\beta^2\left[A_{eq}\frac{\partial^4 W_i}{\partial X^2\partial T^2}+(P_i-P_z-A_{33})\frac{\partial^4 W_i}{\partial X^4}+K_w\left(2\frac{\partial^2 W_i}{\partial X^2}-\frac{\partial^2 W_j}{\partial X^2}\right)\right.$$
$$\left.\left.-K_G\left(\frac{\partial^4 W_i}{\partial X^4}-\frac{\partial^4 W_j}{\partial X^4}\right)+C_d\left(\frac{\partial^3 W_i}{\partial X^2\partial T}-\frac{\partial^3 W_j}{\partial X^2\partial T}\right)\right]\right\}\delta W_i=0, \tag{23}$$

and the non-dimensional boundary conditions come as follows:

$$\left\{D_{eq}\frac{\partial^2 W_i}{\partial X^2}-a_{22}\frac{\partial^2 W_i}{\partial T^2}-\beta^2\left[A_{eq}\frac{\partial^2 W_i}{\partial T^2}+(P_i-P_z-A_{33})\frac{\partial^2 W_i}{\partial X^2}+K_w(2W_i-W_j)-K_G\left(\frac{\partial^2 W_i}{\partial X^2}-\frac{\partial^2 W_j}{\partial X^2}\right)\right.\right.$$
$$\left.\left.+C_d\left(\frac{\partial W_i}{\partial T}-\frac{\partial W_j}{\partial T}\right)\right]\right\}\frac{\partial\delta W_i}{\partial X}\Bigg|_0^1=0, \tag{24a}$$
$$\left\{-D_{eq}\frac{\partial^3 W_i}{\partial X^3}+a_{22}\frac{\partial^3 W_i}{\partial X\partial T^2}+\beta^2\left[A_{eq}\frac{\partial^3 W_i}{\partial X\partial T^2}+(P_i-P_z-A_{33})\frac{\partial^3 W_i}{\partial X^3}+K_w\left(2\frac{\partial W_i}{\partial X}-\frac{\partial W_j}{\partial X}\right)\right.\right.$$
$$\left.\left.-K_G\left(\frac{\partial^3 W_i}{\partial X^3}-\frac{\partial^3 W_j}{\partial X^3}\right)+C_d\left(\frac{\partial^2 W_i}{\partial X\partial T}-\frac{\partial^2 W_j}{\partial X\partial T}\right)\right]+(P_z+A_{33}-P_i(1-\eta))\frac{\partial W_i}{\partial X}\right\}\delta W_i\Bigg|_0^1=0. \tag{24b}$$

3 Solution procedures

3.1 Galerkin approach

The extended Galerkin method is employed to solve the nonlocal governing equations and boundary conditions, and to obtain the eigenvalues of coupled DNBS. The Galerkin method is applied to replace the partial differential equations of motion and related boundary conditions by a finite set of coupled ordinary differential equations. This method considers unknown displacements to the form of the linear combination of trial functions that satisfy convenient boundary conditions. According to this method, the function $W_i(X,T)$ is expressed as follows for the first and second nanobeam:

$$W_i(X,T)=\sum_{r_i=1}^{N_{r_i}}\varphi_{r_i}(X)q_{r_i}(T), \tag{25}$$

where φ_{r_i} is the orthogonal spatial mode functions satisfying the boundary conditions and, q_{r_i} is the generalized coordinates, N_{r_i} denotes the number of modes. Considering a cantilever DNBS, one can use the following family of the orthogonal functions:

$$\varphi_{r_i}(X)=\cosh(\lambda_{r_i}X)-\cos(\lambda_{r_i}X)-\sigma_{r_i}(\sinh(\lambda_{r_i}X)-\sin(\lambda_{r_i}X)),$$
$$\sigma_{r_i}=\frac{\sinh(\lambda_{r_i})-\sin(\lambda_{r_i})}{\cosh(\lambda_{r_i})+\cos(\lambda_{r_i})}. \tag{26}$$

Inserting the displacement fields, eqs. (25), into the governing equations and boundary conditions, eqs. (23) and (24), then taking advantage of the orthogonal properties in the required integrations, the following results are obtained:

$$\begin{bmatrix} \boldsymbol{M}_{11} & \boldsymbol{0} \\ \boldsymbol{0} & \boldsymbol{M}_{22} \end{bmatrix} \ddot{q}(T) + \begin{bmatrix} \boldsymbol{C}_{11} & \boldsymbol{C}_{12} \\ \boldsymbol{C}_{21} & \boldsymbol{C}_{22} \end{bmatrix} \dot{q}(T) + \begin{bmatrix} \boldsymbol{K}_{11} & \boldsymbol{K}_{12} \\ \boldsymbol{K}_{21} & \boldsymbol{K}_{22} \end{bmatrix} q(T) = 0. \tag{27}$$

Also, eq. (27) can be written in compact form as

$$\boldsymbol{M}\ddot{q}(T) + \boldsymbol{C}\dot{q}(T) + \boldsymbol{K}q(T) = 0, \tag{28}$$

where $q(T)$ denotes the overall vector of the generalized coordinates and the dot notation refers to the derivative with respect to time. Also, $\boldsymbol{M}$, $\boldsymbol{C}$ and $\boldsymbol{K}$ are the mass, damping and stiffness matrices, respectively.

3.2 Stability analysis

For the stability analysis, eq. (28) is defined in the first order state-space form

$$\dot{\boldsymbol{Z}}(T) = \boldsymbol{D}\boldsymbol{Z}(T), \tag{29}$$

where the state vector $\boldsymbol{Z}(T)$ is define as

$$\boldsymbol{Z}(T) = \begin{Bmatrix} q(T) \\ \dot{q}(T) \end{Bmatrix} \tag{30}$$

and the state matrix $[D]$ has the form as below:

$$\boldsymbol{D} = \begin{bmatrix} \boldsymbol{0} & \boldsymbol{I} \\ -\boldsymbol{M}^{-1}\boldsymbol{K} & -\boldsymbol{M}^{-1}\boldsymbol{C} \end{bmatrix}, \tag{31}$$

where $[I]$ is the unitary matrix. The solution of eq. (29) has an exponential form that can be written as

$$\boldsymbol{Z} = \overline{\boldsymbol{Z}} \exp(\Omega t). \tag{32}$$

Substituting eqs. (32) into (29) describes a standard eigenvalue problem in the form

$$(\boldsymbol{D} - \Omega \boldsymbol{I})\overline{\boldsymbol{Z}} = 0, \tag{33}$$

in which Ω is the eigenvalue and $\overline{Z}$ presents its corresponding eigenvector. It is obvious from the results that the eigenvalues are generally complex quantities, *i.e.*, $\Omega = \mathrm{Re}(\Omega) + i\,\mathrm{Im}(\Omega)$. As an essential point, it can be noted that the system decaying rate is corresponding to the real part of the eigenvalue while the imaginary part predicts the frequency of the system. To have a nontrivial solution for eq. (33), the determinant of the coefficient matrix vanishes, namely

$$\det(\boldsymbol{D} - \Omega \boldsymbol{I}) = 0. \tag{34}$$

The expansion of the determinant of above equation provides the system characteristic equation. Due to the sign of the real and imaginary parts of complex eigenvalues, the stability and type of instability regions are known [63,64].

4 Results and discussion

In the following section, some numerical results are presented to examine the effects of nonlocal parameter, applied various piezoelectric voltage, surface effects, aspect ratios of length to thickness and the different values of subtangential forces on the vibration and stability behavior of two coupled clamped-free DNBS. The solution of this non-conservative problem via the extended Galerkin approach is considered by eight modes. The geometry, bulk and surface elastic material properties of the system are given in table 1 [65]. Furthermore, the geometric and material constant of PZT-4 piezoelectric actuators are shown in table 1. Moreover, the results are plotted for DNBS with a surrounding elastic medium which is simulated by visco-Pasternak foundation with the following dimensionless properties: $K_w = 20$, $K_G = 1$ and $C_d = 0.5$.

Table 1. The geometric parameters and material surface properties of DNBS integrated with piezoelectric layers [65].

	E (GPa)	ρ (kg/m^3)	L (nm)	b (nm)	h (nm)	ϵ_{33} (N/m^{2}K)	e_{31} (C/m^2)
Nanobeam 1	68.5	2700	200	20	20	–	–
Nanobeam 2	68.5	2700	200	20	20	–	–
Piezoelectric (PZT-4)	78.6	7500	200	20	0.4	1.3×10^{-8}	-9.29
Surface properties (Al)							
λ_s (N/m)		μ_s (N/m),		ρ_s (kg/m^2)		τ_s (N/m)	
6.842		-0.376		5.46×10^{-7}		0.910	

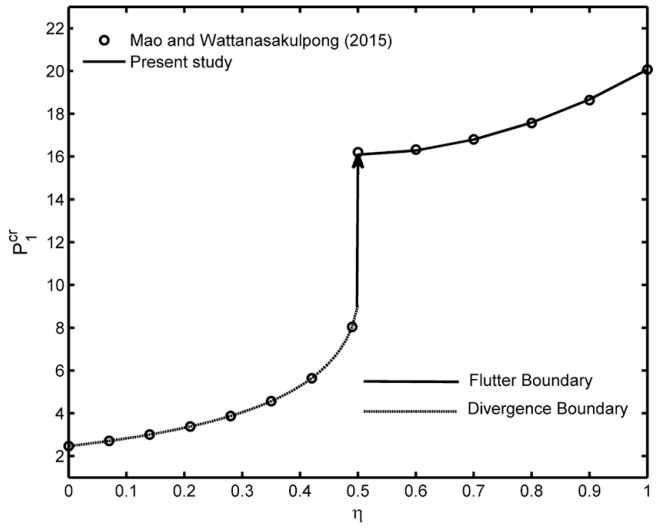

Fig. 2. The validation of divergence and flutter boundaries of DNBS without considering piezoelectric layers and surface effects.

4.1 Validation of the model

In order to justify the validity and applicability of the aforementioned model, the flutter and divergence instability boundaries of cantilever beams are obtained in the absence of the piezoelectric layers, nonlocal parameter and surface effects. The accuracy and applicability of this model is compared with the available results by Mao and Wattanasakulpong [6] in fig. 2. As shown, the current model provides an excellent agreement between the obtained results and the previous result, so the suggested formulation provides a reliable explanation to predict the flutter and divergence instabilities of DNBS. Figure 2 shows the critical instability loads of flutter and divergence *versus* the non-conservative parameter which is considered in the range $0 \leq \eta \leq 1$. As can be seen, by increasing the non-conservative parameter, two types of instability can be observed. The first one is the divergence instability, which is found to occur in the range $0 \leq \eta < 0.5$, while the second one, called the flutter instability, is found in the range $0.5 < \eta \leq 1$. Also, a change in the instability type is observable around $\eta = 0.5$ by means of a sudden jump in the critical load. Furthermore, for both instability types, critical loads increase as the non-conservative parameter, η, increases.

Figures 3(a) and (b) depict the variations of the imaginary and real parts of the two lowest eigenfrequencies with respect to the follower force, respectively. To validate the suggested model, the numerical results of single nanobeam system are presented in fig. 3. It can be demonstrated that the results agree well with those of Kazemi-Lari *et al.* [66] in classical state ($\beta = 0$). However, by increasing the nonlocal parameter β, there is a difference between the results of the present model and those that have been reported by Kazemi-Lari *et al.* [66]. This difference is due to considering the non-classical boundary conditions in the present method, so the predicted values of frequency and critical coupled mode flutter load by this method are higher than those of ref. [66] which considers classical boundary conditions.

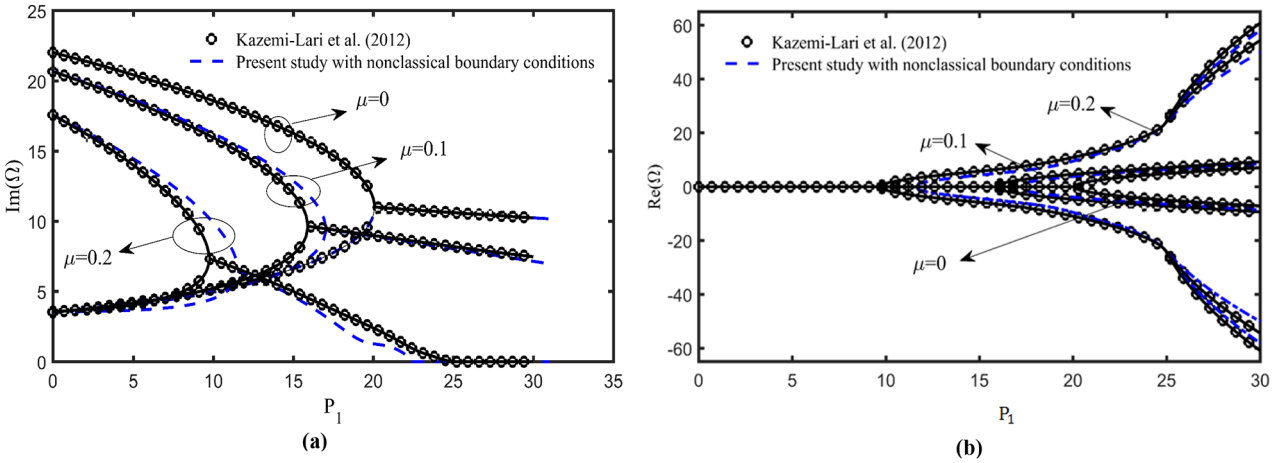

Fig. 3. The validation of two lowest eigenfrequencies of the single nanobeam without considering piezoelectric layers and surface effects: (a) imaginary part, and (b) real part.

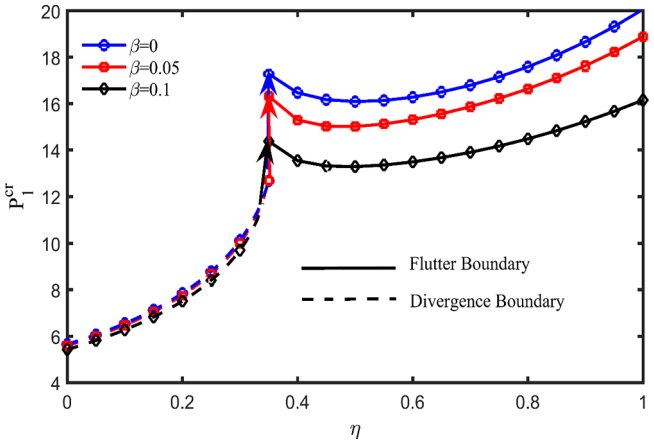

Fig. 4. The effect of the nonlocal parameter on the flutter and divergence boundaries of DNBS without considering piezoelectric layers and surface effects.

4.2 Divergence and flutter analysis

A cantilever DNBS subjected to subtangential forces can undergo different types of instability which strongly depend on the non-conservative parameter. Flutter instability can arise if the non-conservative parameter is considered as $\eta = 1$, however, for purely conservative systems ($\eta = 0$) the instability can only occur by divergence.

4.2.1 The effect of nonlocal parameter

As the small-scale effects play an outstanding role in nanostructures, the classical local continuum theory has not sufficient capacity to describe the mechanical behavior of nanosized materials. Hence, the nonlocal continuum mechanics theory contains information about size dependence and small-scale effects in the elastic solutions of nanostructures, and considers long-range inter-atomic interaction and internal length scale in the construction of constitutive equations. In order to investigate the small-scale effect, fig. 4 is plotted for critical instability forces *versus* the non-conservative parameter with $\frac{P_2}{P_1} = 1$, by considering visco-Pasternak foundation and different nonlocal parameters $\beta = 0, 0.05, 0.1$. Also, the surface effects parameters and piezoelectric voltage are set to zero. In this figure, solid lines are employed to characterize the critical values forces for flutter instability of DNBS, whereas dashed lines are used to indicate those for divergence instability. It is observed that the results of nonlocal elasticity theory predict less flutter and divergence critical loads than the classical continuum theory ($\beta = 0$). Thus, for flutter and divergence instabilities, the critical instability loads decrease when the nonlocal parameter increases. This states that the interaction force between nano-beams atoms reduces along with the increment of the nonlocal parameter, and makes DNBS more flexible than the classical one and consequently, the stability of the system decreases. However, this reduction of the critical flutter instability is much greater than that of the critical divergence instability. Moreover, it can be determined that the small-scale effects cannot be ignored especially for higher nonlocal parameter where the difference between local and nonlocal results is more important. In addition, it can be seen from fig. 4 that depending on the nonlocal parameter, an abrupt jump occurs around $0.33 < \eta < 0.35$ from divergence to flutter instability.

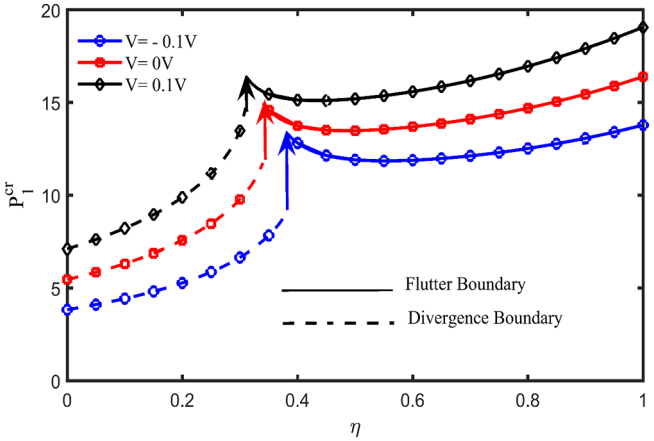

Fig. 5. The effect of applied voltage on the flutter and divergence boundaries of DNBS for $\beta = 0.1$ and without considering surface effects.

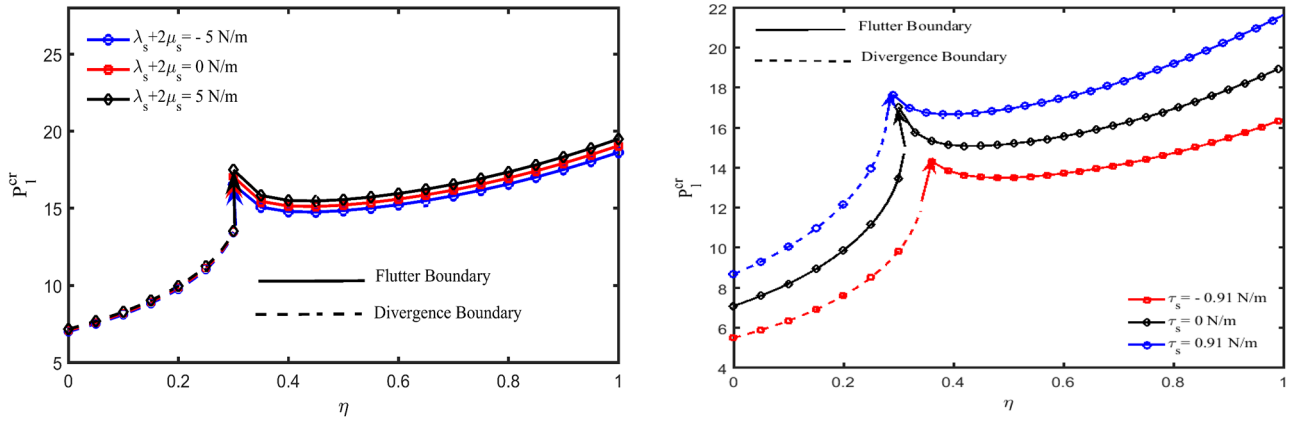

Fig. 6. (a) The effect of the surface elastic constant on the flutter and divergence boundaries of DNBS for $\beta = 0.1$, $V = 0.1\,\mathrm{V}$ and $\tau_s = \rho_s = 0$. (b) The effect of the surface residual stress on the flutter and divergence boundaries of DNBS for $\beta = 0.1$, $V = 0.1\,\mathrm{V}$ and $\lambda_s + 2\mu_s = \rho_s = 0$.

4.2.2 The effect of different piezoelectric voltage

Figure 5 illustrates the critical load as a function of non-conservative parameter for $L/h_b = 10$, $\beta = 0.1$, $\frac{P_2}{P_1} = 1$ and different values of applied voltage without considering surface effects. It is evident that by increasing the piezoelectric voltage from negative to positive, both the divergence and flutter loads increase. Hence, the positive piezoelectric voltage tends to make the DNBS stiffer. For the case of positive piezoelectric voltage, a tensile axial force is induced in the double nanobeams which results in an enhancement in the bending stiffness of the structure. In contrast, when a negative piezoelectric voltage is applied in the direction of the double-nanobeams thickness, a compressive axial force is induced in the DNBS. This reduces the nano-beam bending stiffness. Furthermore, it can be observed that applying the different values of voltage has an important influence on the transition point of divergence to flutter boundaries, in which at higher applied voltages, the critical load jump occurs at lower non-conservative parameter with a decrease in value of jump height between critical divergence and flutter loads. For instance, at a negative applied voltage $V = -0.1\,\mathrm{V}$, a jump in critical load is observed from $P_1^{cr} = 8.99$ to 13.39 near $\eta = 0.4$ while for $V = 0.1\,\mathrm{V}$ jumping occurs at $\eta = 0.31$ from $P_1^{cr} = 14.71$ to 16.42.

4.2.3 The effect of surface layers constant

The effects of surface elastic constants, $\lambda_s+2\mu_s$, on the critical loads of DNBS are illustrated in fig. 6(a) with considering $\rho_s = \tau_s = 0$, $\beta = 0.1$, $V = 0.1\,\mathrm{V}$ and $\frac{P_2}{P_1} = 1$. It is observed that unlike the negative surface elastic constant, which makes the system softer, the positive one predicts more critical flutter and divergence loads. Therefore, the system may be stiffer or softer depending on the sign of the surface elastic constant. Also, it can be seen that the surface elastic constants have considerable influence on the flutter boundary, but not on the divergence boundary. It is evident that the abrupt jump from divergence to flutter boundary takes place at the same value of the non-conservative parameter

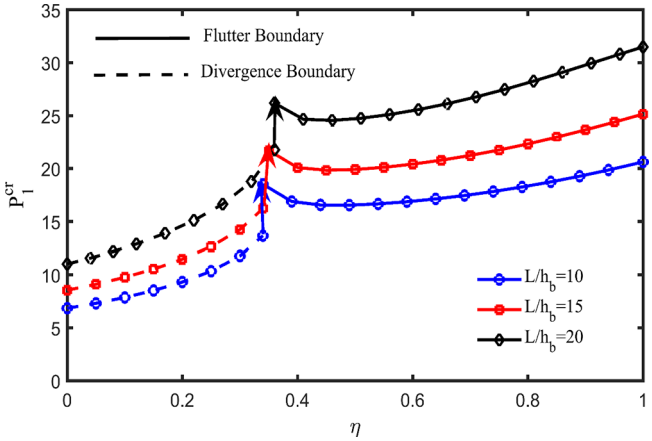

Fig. 7. The effect of the aspect ratio on the flutter and divergence boundaries of DNBS considering surface effects for $\beta = 0.1$ and $V = 0.1\,\mathrm{V}$.

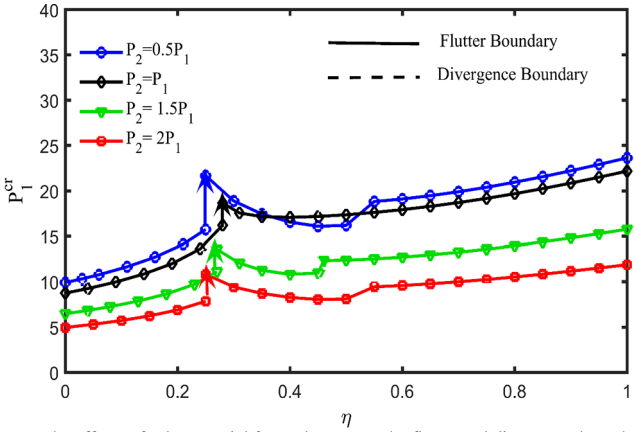

Fig. 8. The effects of subtangential force changes on the flutter and divergence boundaries of DNBS considering surface effects for $\beta = 0.1$ and $V = 0.1\,\mathrm{V}$.

($\eta = 0.3$) for different surface elastic constants. Figure 6(b) indicates the influence of surface residual stress on the critical instability loads for variations of the non-conservative parameter. The values of $\lambda_s + 2\mu_s$ and ρ_s are set to zero, and $\beta = 0.1$, $V = 0.1\,\mathrm{V}$ and $\frac{P_2}{P_1} = 1$ are considered. From fig. 6(b), it can be seen that a positive residual surface stress ($\tau_s > 0$) results in a positive distributed force or the existence of tensile stress in the structure, which increases the critical load of the DNBS (vice versa for $\tau_s < 0$). So that, it is found that the change of values of the surface residual stress from negative to positive, increases the flutter and divergence loads and makes the system more stable. Also, it can be noted that the critical instability loads are strongly affected by the surface residual stress. As can be seen, the abrupt jump from divergence to flutter boundary takes place at different values of the non-conservative parameter. Although it is not shown here, the surface density does not have significant influence on the divergence and flutter boundaries.

4.2.4 The effect of the aspect ratio

To illustrate the effect of the aspect ratio, L/h_b, the stability map of the DNBS in the η-P_1^{cr} plane is plotted in fig. 7. The critical loads are calculated for the three different values of the aspect ratio, $L/h_b = 10, 15$ and 20 with considering surface effects, visco-Pasternak foundation, $\beta = 0.1$ and $V = 0.1\,\mathrm{V}$. It can be observed that the divergence and flutter loads increase as the aspect ratio increases. So that, a large value of the aspect ratio predicts more critical loads and consequently, increases the stability of the system. In addition, the results show that increasing the aspect ratio does not have a significant influence on the transition point position, in other words, the jump point is approximately in the range $0.34 < \eta < 0.36$.

4.2.5 The effect of the variation of the subtangential force

Taking the surface effects into consideration, the effect of the subtangential force on the critical load of DNBS with respect to the non-conservative parameter is shown in fig. 8. In this case, the nonlocal parameter and piezoelectric voltage are assumed as $\beta = 0.1$ and $V = 0.1\,\mathrm{V}$, respectively. It is obvious that by increasing the subtangential force

Table 2. The effect of the nonlocal parameter on the two lowest eigenfrequencies of DNBS without considering surface effects, $P_2 = P_1 = 5$ and $V = 0\,\mathrm{V}$.

β	$\eta = 0$		$\eta = 0.3$		$\eta = 0.6$		$\eta = 1$	
	Ω_1	Ω_2	Ω_1	Ω_2	Ω_1	Ω_2	Ω_1	Ω_2
0	0.0000+	−0.4945+	0.0000+	−0.4945+	0.0000+	−0.4945+	0.0000+	−0.4945+
	2.2039i	6.3292i	4.1237i	7.2575i	5.1905i	7.9449i	6.1258i	8.6257i
0.05	0.0000+	−0.4981+	0.0000+	−0.4963+	0.0000+	−0.4946+	0.0000+	−0.4927+
	2.1330i	6.3039i	4.1115i	7.2456i	5.1882i	7.9325i	6.1222i	8.6037i
0.1	0.0000+	−0.5116+	0.0000+	−0.5048+	0.0000+	−0.4984+	0.0000+	−0.4911+
	1.8915i	6.2218i	4.0775i	7.2137i	5.1851i	7.9041i	6.1132i	8.5506i

Table 3. The effect of the piezoelectric voltage on the two lowest eigenfrequencies of DNBS considering surface effects, $\beta = 0.1$ $P_2 = P_1 = 2$ and $L/h_b = 10$.

$V(V)$	$\eta = 0$		$\eta = 0.3$		$\eta = 0.6$		$\eta = 1$	
	Ω_1	Ω_2	Ω_1	Ω_2	Ω_1	Ω_2	Ω_1	Ω_2
−0.2	0.0000+	−0.50206+	0.0000+	−0.49938+	0.0000+	−0.4968+	0.0000+	−0.4935+
	3.5814i	6.9646i	4.1664i	7.2909i	4.6382i	7.5766i	5.1505i	7.9066i
−0.1	0.0000+	−0.50208+	0.0000+	−0.4995+	0.0000+	−0.4970+	0.0000+	−0.4939+
	4.6917i	7.6764i	5.0778i	7.9238i	5.4104i	8.1448i	5.7903i	8.4052i
0	0.0000+	−0.5017+	0.0000+	−0.49934+	0.0000+	−0.4970+	0.0000+	−0.4940+
	5.4862i	8.2516i	5.7726i	8.4475i	6.0272i	8.6252i	6.3265i	8.8376i
0.1	0.0000+	−0.5013+	0.0000+	−0.4990+	0.0000+	−0.4968+	0.0000+	−0.4941+
	6.1192i	8.7387i	6.3451i	8.8989i	6.5499i	9.0458i	6.7952i	9.2235i
0.2	0.0000+	−0.5008+	0.0000+	−0.4987+	0.0000+	−0.4966+	0.0000+	−0.49414+
	6.6539i	9.1651i	6.8393i	9.2994i	7.0097i	9.4235i	7.2165i	9.5753i

ratio, $\frac{P_2}{P_1}$, from 0.5 to 2, the critical divergence and flutter loads decrease. Generally, the stability region of the system reduces as $\frac{P_2}{P_1}$ increases. In other words, increasing $\frac{P_2}{P_1}$ causes to apply more loads to the DNBS and results in reducing the stiffness of the system and the stable area. Depending on the values of the non-conservative parameters, flutter can be caused by the coalescence of different structural modes. For instance, when $\frac{P_2}{P_1} = 0.5$, in the range $0.25 < \eta < 0.52$, the flutter instability of the cantilevered DNBS will occur when the imaginary parts of the first and second eigenvalue modes coalesce. Increasing the non-conservative parameter η, flutter instability occurs due to the coalescence of the second and third eigenvalue modes. Therefore, a jump is observed around $\eta = 0.52$.

4.3 Frequency analysis

The vibrational frequencies of DNBS under the action of subtangential forces are investigated in this subsection. Here, the influences of non-conservative and nonlocal parameters, piezoelectric layer's voltage, surface parameters and aspect ratio on the two lowest frequencies Ω_1 and Ω_2 are examined in detail. The effect of different nonlocal parameters without considering the piezoelectric voltage and surface effects, and $P_1 = P_2 = 5$ on the real and imaginary parts of the first two eigenfrequencies is presented in table 2. It can be seen that by increasing the value of the nonlocal parameter, both the first and second natural frequencies decrease for each value of the non-conservative parameter.

The results in table 3 are reported in terms of the first two lowest eigenfrequencies for the various values of the applied voltage and non-conservative parameter for $\beta = 0.1$, $P_1 = P_2 = 2$ and $L/h_b = 10$ with considering surface effects. It is shown that increasing the piezoelectric layers voltage from $V = -0.2\,\mathrm{V}$ to $0.2\,\mathrm{V}$ (same as η increased) leads to an increase in the first and second modes of the frequencies. It can be concluded from table 3, that the positive voltage increases the stiffness of the system.

Table 4. The effect of the surface residual stress on the two lowest eigenfrequencies of DNBS considering $\beta = 0.1$, $V = 0.1\,\mathrm{V}$, $\rho_s = \mu_s = \lambda_s = 0$, $P_2 = P_1 = 2$ and $L/h_b = 10$.

τ_s	$\eta = 0$		$\eta = 0.5$		$\eta = 1$	
	Ω_1	Ω_2	Ω_1	Ω_2	Ω_1	Ω_2
-0.6	0.0000+	-0.5123+	0.0000+	-0.5079+	0.0000+	-0.5039+
	5.0312i	7.9614i	5.5865i	8.3300i	6.0334i	8.6390i
0	0.0000+	-0.5121+	0.0000+	-0.5079+	0.0000+	-0.5040+
	5.5248i	8.3249i	5.9885i	8.6433i	6.3720i	8.9141i
0.6	0.0000+	-0.5118+	0.0000+	-0.5077+	0.0000+	-0.5040+
	5.9512i	8.6510i	6.3478i	8.9297i	6.6826i	9.1696i

Table 5. The effect of surface elastic constant on the two lowest eigenfrequencies of DNBS considering $\beta = 0.1$, $V = 0.1\,\mathrm{V}$, $\rho_s = \tau_s = 0$, $P_2 = P_1 = 2$ and $L/h_b = 10$.

$\lambda_s + 2\mu_s$	$\eta = 0$		$\eta = 0.5$		$\eta = 1$	
	Ω_1	Ω_2	Ω_1	Ω_2	Ω_1	Ω_2
-5	0.0000+	-0.5124+	0.0000+	-0.5081+	0.0000+	-0.5041+
	5.4950i	8.3060i	5.9609i	8.6251i	6.3447i	8.8956i
0	0.0000+	-0.5121+	0.0000+	-0.5079+	0.0000+	-0.5040+
	5.5248i	8.3249i	5.9885i	8.6433i	6.3720i	8.9141i
5	0.0000+	-0.5118+	0.0000+	-0.5077+	0.0000+	-0.5039+
	5.5545i	8.3439i	6.0160i	8.6615i	6.3991i	8.9326i

Table 6. The effect of the aspect ratio on the two lowest eigenfrequencies of DNBS considering surface effects, $\beta = 0.1$, $V = 0.1\,\mathrm{V}$ and $P_2 = P_1 = 2$.

$\frac{L}{h_b}$	$\eta = 0$		$\eta = 0.5$		$\eta = 1$	
	Ω_1	Ω_2	Ω_1	Ω_2	Ω_1	Ω_2
10	0.0000+	-0.5013+	0.0000+	-0.4975+	0.0000+	-0.4941+
	6.1192i	8.7387i	6.4838i	8.9982i	6.7952i	9.2235i
20	0.0000+	-0.4984+	0.0000+	-0.4958+	0.0000+	-0.4934+
	8.5985i	10.7911i	8.7539i	10.9060i	8.8967i	11.0115i
50	0.0000+	-0.4931+	0.0000+	-0.4923+	0.0000+	-0.4916+
	16.7687i	18.2434i	6.7983i	18.2603i	16.8273i	18.2769i

The non-dimensional natural frequencies corresponding to the two lowest eigenfrequencies of DNBS are presented in tables 4 and 5 with respect to surface residual stress and surface elastic constants, respectively. Here, $\beta = 0.1$, $V = 0.1\,\mathrm{V}$ and $L/h_b = 10$ are assumed. The data would seem to suggest that applying negative/positive surface residual stress decreases/increases the natural eigenfrequencies. The results of table 5 show that the eigenfrequencies of the DNBS increase, as $\lambda_s + 2\mu_s$ increases. The influence of the value of the aspect ratio on the vibrational behavior of DNBS is indicated in table 6 with considering surface effects. Here the results are obtained for the value $\beta = 0.1$, $V = 0.1\,\mathrm{V}$. As can be seen from table 6, by increasing the value of the aspect ratio, the first two natural frequencies of the system increase.

5 Conclusion

On the basis of Eringen's nonlocal and Gurtin-Murdoch continuum elasticity theories, the general equations for free vibration of the cantilever DNBS subjected to subtangential forces in conjunction with a surrounding elastic medium were computed. Using the extended Hamilton's principle, the nonlocal governing equations of motion and corresponding boundary conditions were derived. The extended Galerkin method is employed to obtain the numerical solutions and the eigenvalues of the model. The vibration characteristics of coupled DNBS were explained and the effects of nonlocal and non-conservative parameters, piezoelectric layer's voltage, surface effects and aspect ratio on the divergence and flutter boundaries of the system are comprehensively described. According to the obtained results, the stability of system decreases as the nonlocal parameter increases. Additionally, the results indicated that by increasing the applied voltage and surface effects from negative to positive values, the critical divergence and flutter loads increase. Also, the increasing of the aspect ratio and force factor ratio resulted in the increment and decrement of the critical loads, respectively. Hence, a set of physical and design parameters are important factors in affecting the eigenvalues and instability boundaries of the DNBS.

References

1. Q.H. Zuo, H.L. Schreyer, Int. J. Solids Struct. **33**, 1355 (1996).
2. M.A. Langthjem, Y. Sugiyama, Comp. Struct. **74**, 385 (2000).
3. M.A. Langthjem, Y. Sugiyama, Comp. Struct. **74**, 399 (2000).
4. Z. Elfelsoufi, L. Azrar, Comp. Struct. **83**, 2632 (2005).
5. M. Şimşek, S. Cansız, Compos. Struct. **94**, 2861 (2012).
6. Q. Mao, N. Wattanasakulpong, Int. J. Mech. Sci. **93**, 1 (2015).
7. Y.Q. Zhang, Y. Lu, G.W. Ma, Int. J. Mech. Sci. **50**, 299 (2008).
8. S. Caddemi, I. Caliò, F. Cannizzaro, J. Sound Vib. **333**, 1718 (2014).
9. N.I. Kim, J. Lee, Int. J. Mech. Sci. **84**, 91 (2014).
10. H.S. Alkhaldi, I. Abu-Alshaikh, R. Abu-Mallouh, O. Ghazal, Eur. J. Mech. A **47**, 271 (2014) (Supplement C).
11. X.F. Li, J. Zou, S.N. Jiang, K.Y. Lee, Compos. Struct. **153**, 645 (2016).
12. R. Bahaadini, M. Hosseini, B. Jamali, Physica B: Condens. Matter **529**, 57 (2018) (Supplement C).
13. M. Sadeghi-Goughari, M. Hosseini, J. Mech. Sci. Technol. **29**, 723 (2015).
14. M. Hosseini, M. Sadeghi-Goughari, Appl. Math. Model. **40**, 2560 (2016).
15. R. Bahaadini, M.R. Dashtbayazi, M. Hosseini, Z. Khalili-Parizi, Ocean Eng. **160**, 311 (2018).
16. R. Bahaadini, A.R. Saidi, Eur. J. Mech. - A **72**, 298 (2018).
17. R. Bahaadini, A.R. Saidi, Aerospace Sci. Technol. **80**, 381 (2018).
18. R. Bahaadini, A.R. Saidi, Thin-Walled Struct. **132**, 604 (2018).
19. A.C. Eringen, J. Appl. Phys. **54**, 4703 (1983).
20. M.E. Gurtin, A.I. Murdoch, Int. J. Solids Struct. **14**, 431 (1978).
21. F. Ebrahimi, M. Reza Barati, Eur. Phys. J. Plus **132**, 19 (2017).
22. R.A. Toupin, Arch. Ration. Mech. Anal. **11**, 385 (1962).
23. B. Alibeigi, Y. Tadi Beni, F. Mehralian, Eur. Phys. J. Plus **133**, 133 (2018).
24. E.C. Aifantis, Int. J. Fract. **95**, 299 (1999).
25. B. Alibeigi, Y. Tadi Beni, Eur. Phys. J. Plus **133**, 398 (2018).
26. C.W. Lim, G. Zhang, J.N. Reddy, J. Mech. Phys. Solids **78**, 298 (2015).
27. J.N. Reddy, Int. J. Eng. Sci. **45**, 288 (2007).
28. R. Bahaadini, M. Hosseini, Comp. Mater. Sci. **114**, 151 (2016).
29. Q. Wang, K.M. Liew, Phys. Lett. A **363**, 236 (2007).
30. T. Murmu, S. Adhikari, Phys. Lett. A **375**, 601 (2011).
31. R. Bahaadini, M. Hosseini, Appl. Math. Model. **59**, 597 (2018).
32. A. Ghorbanpour Arani, M.A. Roudbari, K. Kiani, Mech. Adv. Mater. Struct. **23**, 281 (2016).
33. M. Hosseini, R. Bahaadini, M. Makkiabadi, Microfluid. Nanofluid. **22**, 6 (2018).
34. M. Hosseini, M. Sadeghi-Goughari, S. Atashipour, M. Eftekhari, Arch. Mech. **66**, 217 (2014).
35. F. Ebrahimi, M.R. Barati, J. Vib. Control **24**, 549 (2016).
36. A. Jamalpoor, A. Ahmadi-Savadkoohi, M. Hosseini, S. Hosseini-Hashemi, Eur. J. Mech. A **63**, 84 (2017) (Supplement C).
37. R. Omidian, Y. Tadi Beni, F. Mehralian, Eur. Phys. J. Plus **132**, 481 (2017).
38. A.H. Ghorbanpour Arani, A. Rastgoo, A. Hafizi Bidgoli, R. Kolahchi, A. Ghorbanpour Arani, Mech. Adv. Mater. Struct. **24**, 1159 (2017).
39. O. Rahmani, S. Norouzi, H. Golmohammadi, S.A.H. Hosseini, Mech. Adv. Mater. Struct. **24**, 1274 (2017).
40. R. Bahaadini, A.R. Saidi, M. Hosseini, Int. J. Eng. Sci. **123**, 181 (2018).

41. M. Atashafrooz, R. Bahaadini, H.R. Sheibani, Mech. Adv. Mater. Struct., 1 (2018).
42. R. Bahaadini, A.R. Saidi, M. Hosseini, J. Vib. Control **25**, 203 (2019).
43. T. Murmu, J. Sienz, S. Adhikari, C. Arnold, J. Appl. Phys. **110**, 084316 (2011).
44. F. Ebrahimi, M.R. Barati, Eur. Phys. J. Plus **131**, 346 (2016).
45. A. Ciekot, S. Kukla, J. Appl. Math. Comput. Mech. **13**, 23 (2014).
46. M. Hosseini, A.Z.B. Maryam, R. Bahaadini, Microfluid. Nanofluid. **21**, 134 (2017).
47. X.F. Li, S.N. Jiang, K. Lee, Int. J. Mech. Mater. Design **14**, 91 (2018).
48. R. Bahaadini, M. Hosseini, A. Jamalpoor, Physica B: Condens. Matter **509**, 55 (2017).
49. S. Narendar, S. Ravinder, S. Gopalakrishnan, Comp. Mater. Sci. **56**, 179 (2012).
50. X. Chen, C.Q. Fang, X. Wang, Physica E **85**, 47 (2017).
51. Y. Zhang, M. Pang, L. Fan, Phys. Lett. A **380**, 2294 (2016).
52. K. Kiani, Physica E **86**, 225 (2017).
53. K. Liao-Liang, W. Yue-Sheng, Smart Mater. Struct. **21**, 025018 (2012).
54. Y. Zhi, J. Liying, J. Phys. D **46**, 355502 (2013).
55. M. Hosseini, R. Bahaadini, B. Jamali, J. Vib. Control **24**, 1809 (2018).
56. A. Fereidoon, E. Andalib, A. Mirafzal, Physica E **81**, 205 (2016) (Supplement C).
57. A. Ghorbanpour-Arani, A. Rastgoo, M. Sharafi, R. Kolahchi, A.G. Arani, Meccanica **51**, 25 (2016).
58. A.C. Eringen, D.G.B. Edelen, Int. J. Eng. Sci. **10**, 233 (1972).
59. Z.G. Zhou, L.Z. Wu, S.Y. Du, Eur. J. Mech. A **25**, 793 (2006).
60. M.E. Gurtin, A.I. Murdoch, Arch. Ration. Mech. Anal. **57**, 291 (1975).
61. P. Lu, L. He, H. Lee, C. Lu, Int. J. Solids Struct. **43**, 4631 (2006).
62. G. Rezazadeh, A. Tahmasebi, M. Zubstov, Microsyst. Technol. **12**, 1163 (2006).
63. M. Hosseini, S.A. Fazelzadeh, Int. J. Struct. Stabil. Dyn. **11**, 513 (2011).
64. M. Hosseini, R. Bahaadini, Int. J. Eng. Sci. **101**, 1 (2016).
65. R. Ansari, A. Norouzzadeh, R. Gholami, M.F. Shojaei, M. Darabi, Microfluid. Nanofluid. **20**, 1 (2016).
66. M. Kazemi-Lari, S.A. Fazelzadeh, E. Ghavanloo, Physica E **44**, 1623 (2012).